



Biodegradable iron-based foams prepared by the space holder technique using urea

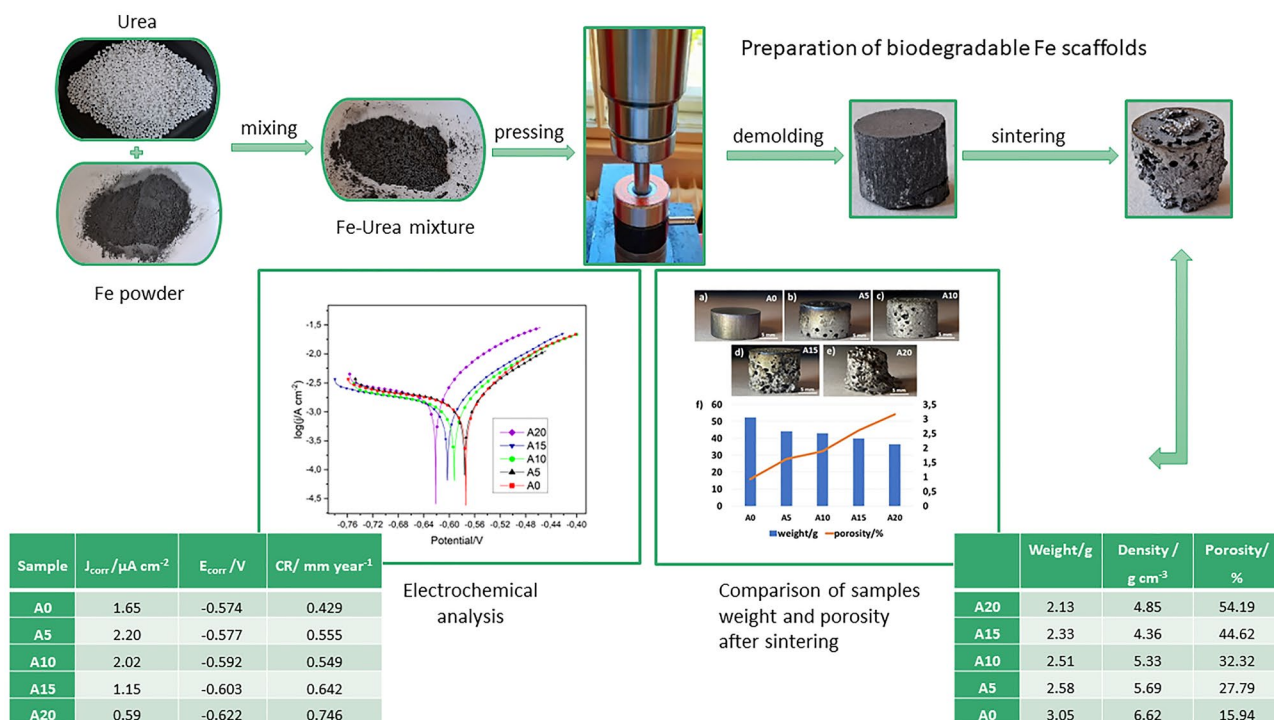
V. Čákyová¹ · R. Gorejová^{1,2} · R. Macko¹ · O. Petruš³ · T. Sopčák³ · M. Kupková³ · F. Kaňavský¹ · R. Oriňaková^{1,2}

Received: 17 May 2023 / Accepted: 15 September 2023
 © The Author(s) 2023

Abstract

Iron-based degradable biomaterials have attracted much attention as next-generation bone implants due to their excellent mechanical properties and good biocompatibility. Many studies are now focusing on the preparation and detailed study of porous versus non-porous degradable materials. Porous degradable biomaterials have many advantages over the non-porous ones owing to their structure, which allows easier bone tissue ingrowth. The aim of this work was to prepare Fe-based biodegradable porous materials in a cost-effective way via powder metallurgy technique using urea space holders. Five different samples with increasing space holder weight ratio (up to 20 wt%) were prepared. Surface morphology and sample structure were studied using the optical microscopy, Raman spectroscopy, and scanning electron microscopy (SEM) with energy-dispersive X-ray analysis (EDX). Electrochemical corrosion rate analysis confirmed that the samples corroded faster with increasing number of pores. With an increasing amount of urea, the number of pores increased proportionally, which can potentially be used to tune the corrosion rate. However, mechanical integrity of the samples was not maintained when more than 10 wt% of space holder was used.

Graphical abstract



Extended author information available on the last page of the article

Keywords Space holder · Urea · Iron foam · Biodegradation · Corrosion

1 Introduction

In the past few decades, huge advantages have been made in medical care leading to an increase in the quality of life and average lifespan of humans. With the growing average length of a human's life, there is an increasing need for the use of orthopaedic implants [1, 2]. An orthopaedic implant can be defined as a device designed to restore function by replacing or reinforcing a damaged structure [3]. Although traditional (inert) biomaterials have been used as orthopaedic implants for many decades, there are still many problems (implant loosening, design errors, effusions, infection-mimicking reactions, allergic reactions, impaired wound, and fracture healing, second surgery to remove screws and plates) with their use often leading to implant failure [4, 5]. If the implant fails, second surgery is required to remove it, which poses risk to the patient, prolongs their recovery, and puts a financial burden on the patient and hospitals. Therefore, in the last decade, research has begun to focus on biodegradable implants, which have the potential to reduce the need for a second surgery and minimize the incidence of infection associated with implantation [6–9].

Biodegradable implants are made of biodegradable metals, which can be defined as metals that are expected to gradually corrode in vivo with an appropriate host response to the released corrosion products and, after performing their function of supporting the tissue while healing, they completely dissolve with no implant residue. The most widely used biodegradable metals include Fe-based alloys, Mg-based alloys, and Zn-based alloys [2, 10–17]. Fe plays an important role in the metabolism of the human body, including transport, activation, and storage of molecular oxygen, reduction of ribonucleotides and dinitrogen, and degradation of lipids, proteins, and DNA. Fe-based materials have remarkable mechanical properties (similar to stainless steel) and great biodegradability making Fe an ideal choice for load-bearing applications [2, 18, 19].

The microstructure and mechanical properties of materials can be directly affected by processing methods. In this study, two methods were used to influence the structure: powder metallurgy and the use of space holders. Porous metallic biomaterials show several improved properties compared to structurally unmodified biomaterials. These include lower weight, larger surface area, higher hardness, and lower thermal conductivity [20–25]. Also, porous materials can mimic the structure and mechanical properties (reduction of Young's modulus and therefore possible stress

shielding effect prevention) of natural tissues such as bone more closely, as well as enhance tissue regeneration, integration, proper vascularization, and tissue ingrowth. Because of the pores, the cells can grow through these biomaterials and thereby promote cell infiltration, proliferation, and differentiation. Moreover, pores allow many material functions like inward dispersion of oxygen, nutrients, analytes, and outward diffusion of pharmaceutical agents, angiogenesis, and pro-healing responses from immune cells that can affect foreign body reactions. One of the suitable methods for production of these substances is the space holder method. Powder-based techniques use two types of space holders that are removed differently. The first category is removed by dissolution, which is represented mainly by NaCl [26–28]. The second category is removed by evaporation or combustion while the powder preform is heated to its sintering temperature. This category is mainly represented by urea, which can be removed by heating above 200 °C. The advantage of using the second category is that the shrinkage of the sintering metal is not blocked by the space holder. Powder metallurgy techniques can be more cost-effective than other techniques like additive manufacturing or casting. These methods often include the need for expensive specialized equipment, software, and skilled professionals. The cost of powder metallurgy depends on the input material—the complexity, the size, and the quantity. Since iron is one of the most affordable metals and urea particles are also inexpensive, the preparation of Fe-based biodegradable porous materials via this method can be considered cost-effective [29–31]. In this study, we fabricated porous Fe biodegradable materials by a powder metallurgy method using urea as a space holder. We managed to prepare affordable porous Fe materials with different porosities by using different weight ratios of urea, which was the main aim of this study.

2 Materials and methods

2.1 Sample preparation

Iron (Fe) powder (spherical, < 10 micron, 99.9+% (metals basis), 99.5%, Alfa Aesar, Germany) was used for the preparation of porous samples and urea (analytical grade, Centralchem, Slovakia) was used as a space holder. These two components (Fe and urea) were mixed in a weight ratio of 100:0, 95:5, 90:10, 85:15, and 80:20. The samples were labelled as A0, A5, A10, A15, and A20 where the

number represents the urea content in weight per cent. A bare Fe sample was used as a reference. Mixture was mechanically mixed and then homogenized in a Turbula mixing machine for 1 h to prepare a mixture with evenly distributed urea (Ur) and Fe particles. To fabricate the samples, 5 g of each mixture was pressed into a cylindrical shape (12 mm Ø) using hydraulic press with a pressure of 400 MPa and then sintered in two steps using Carbolite tube furnace (Carbolite Gero, United Kingdom). During the first step, the samples were sintered at 200 °C for 4 h in a nitrogen atmosphere to remove urea. The furnace heating rate was 5 °C per minute. Subsequently, the samples were cooled down to a room temperature. In the second step, samples were sintered at 1120 °C for 1 h in a reducing hydrogen atmosphere [32, 33]. The heating rate was 10 °C per minute.

2.2 Sample characterization

2.2.1 Morphology and microstructure

Optical microscopy was used to study samples morphology (Dino-Lite Premier AM4013MT, Dino-Lite AM4815ZT and Dino-Lite AM4515T8, ~20–900× magnification, 1.3 MPx, Dino-Lite, Delmenhorst Netherlands). For detailed microstructural analysis, scanning electron microscopy (SEM, JEOL JSM-7001F, Jeol Ltd., Tokyo, Japan) with energy-dispersive X-ray analysis (EDX) (INCA EDX analyzer, Oxford Instruments, Abingdon, Oxfordshire, United Kingdom) was used. Raman spectroscopy was performed with an XploRA ONE spectrometer (Horiba Yvon Jobin, France) with a 50 mW (original laser power) 532 nm laser source. Spectral data were collected using a ×100 microscope objective over the range of 200–1800 cm⁻¹ with a 5 s acquisition time, 3 accumulations, and 10% of original laser power.

2.2.2 Electrochemical tests

The electrochemical tests were performed using the Autolab PGSTAT 302N potentiostat (Metrohm AG, Switzerland) in a three-electrode set-up consisting of a reference silver chloride (Ag/AgCl/KCl 0.1 M) electrode, a platinum (Pt) electrode, and sample (working electrode). The tests were performed in 50 ml of Hanks' solution (8 g dm⁻³ NaCl, 0.4 g dm⁻³ KCl, 0.14 g dm⁻³ CaCl₂, 0.06 g dm⁻³ MgSO₄·7H₂O, 0.06 g dm⁻³ NaH₂PO₄·2H₂O, 0.35 g dm⁻³ NaHCO₃, 1.00 g dm⁻³ glucose, 0.60 g dm⁻³ KH₂PO₄, and 0.10 g dm⁻³ MgCl₂·6H₂O) which simulated the human body

conditions. The system was heated to a constant temperature of 37 ± 2 °C. Before the measurements, samples were cleaned in acetone and ethanol for 5 min using an ultrasonic cleaner (Ultrasonic Laboratory 6, ULTRAZVUK, Czech Republic). The open circuit potential (OCP) was recorded for 1 h to reach the equilibrium before the corrosion measurements. After the OCP measurement, the corrosion rate was determined from potentiodynamic polarization curves acquired in the range between OCP – 0.2 V and OCP + 0.2 V at scanning rate of 0.1 mV s⁻¹ and evaluated by the Tafel extrapolation method. The corrosion rate was calculated from Eq. (1):

$$CR = \frac{j_{\text{corr}}KEW}{d} \quad (1)$$

where CR stands for corrosion rate (mm year⁻¹), j_{corr} is corrosion current density (μA cm⁻²), K is a constant (3.27 × 10⁻³) determining CR units, EW is equivalent weight of iron (27.92 g eq⁻¹), and d is the density of the measured sample [34].

2.2.3 Determination of density, porosity, and elasticity

Specimen density was calculated by the Archimedes principle according to ISO3369. The samples were wrapped in Parafilm and then weighed in air and water, and density was calculated according to Eq. (2):

$$d = \frac{m_1}{\frac{(m_{1P}-m_{2P})}{d_w} - \frac{(m_{1P}-m_1)}{d_p}} \quad (2)$$

where m_1 (g) is the weight of the dry samples not wrapped in Parafilm (P), m_{1P} (g) stands for the weight of the samples wrapped in Parafilm and weighed in air, m_{2P} (g) represents the weight of the wrapped specimens weighed in water, d_w (g cm⁻³) is the density of water at room temperature (g cm⁻³), and d_p (g cm⁻³) is the density of the Parafilm (g cm⁻³).

The samples were soaked with benzyl alcohol in a vacuum and subsequently weighed in air and water for total porosity (P_T) determination which was calculated according to the Eq. (3):

$$P_T = 1 - \frac{m_1}{(m_2 - m_3)\gamma} \times 100 \quad (3)$$

where m_1 (g) is the weight of the dried specimens before saturation, m_2 (g) stands for the weight of the benzyl alcohol saturated specimens, m_3 (g) stands for the weight of the saturated specimens weighed in water, and γ (g cm⁻³) is the theoretical density of metal [35].

The dynamic resonant method was used to evaluate the modulus of elasticity (E). The natural frequency of the fundamental bending mode was measured utilizing the equipment BUZZ-O-SONIC 5.9.6. (BuzzMac International, LLC, U.S.A), and the corresponding modulus of elasticity was calculated by the equipment software.

3 Results

3.1 Metallic foam characterization

Iron powder and urea (Fig. 1a) used as a space holder were mixed in ratios of 100:0, 95:5, 90:10, 85:15, and 80:20 wt%. A cylindrical die was used during the moulding process to achieve a uniform shape of the samples. Before sintering, the samples were cylindrical (diameter of 12 mm, height of 3.8 mm). The urea particles were coated with a layer of iron powder (Fig. 1b) and retained their spherical shape even after compression. After the sintering process, the urea was removed, leaving behind pores of different sizes (Fig. 2a–e). The cylindrical shape of the samples was retained, but in the case of higher additions of space holders (more than 10 wt%), the samples did not maintain compactness (Fig. 2d, e).

The porosity, weight, and density of the materials were also monitored and determined after sintering (Fig. 2f). Due to the manual preparation of the samples, the weights of the individual samples were not identical and varied from 2.13 to 3.05 g per sample. The density of the samples was 6.62 g cm^{-3} for the A0, 5.69 g cm^{-3} for the A5, 5.33 g cm^{-3} for the A10, 4.36 g cm^{-3} for the A15, and 4.85 g cm^{-3} for the A20 sample, respectively. Figure 2f also confirms the inverse proportionality between the weight and the porosity of the samples. As the urea content increased, the number of pores increased as well.

The inverse proportionality between the weight of the samples and their porosity is evident also from Fig. 2a–e, in which the optical images of the individual samples after sintering are shown. For the sample A20, the ratio is

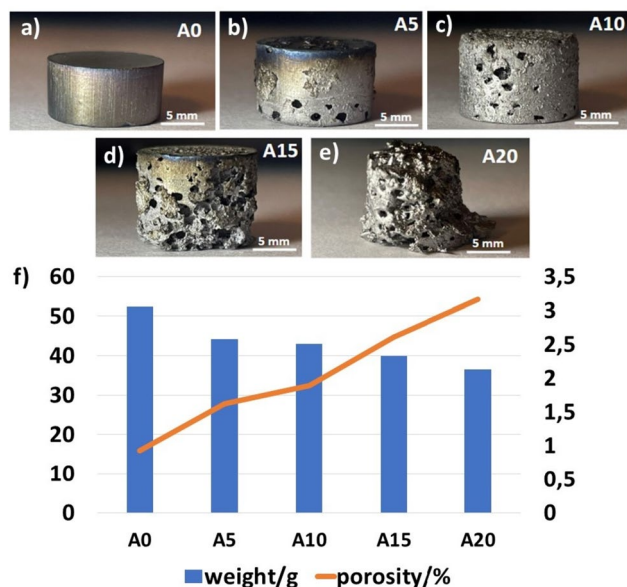


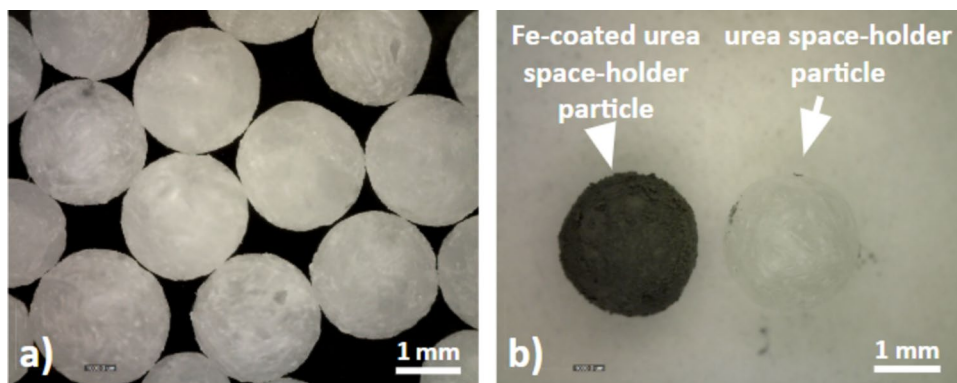
Fig. 2 Macroscopic images of the sintered cylindrical samples with 0 (a), 5 (b), 10 (c), 15 (d), and 20 (e) urea space holder weight percentage. Comparison of samples weight and porosity after sintering (f)

approaching a threshold value, beyond which the samples begin to completely disintegrate.

The surface morphology of the prepared samples was evaluated by scanning electron microscopy (Fig. 3). The gradual increase in surface roughness can be attributed to the absence of material, due to the removal of the urea, which left an empty space. The difference in porosity between the prepared samples can also be observed in Fig. 3a–e, where the details of the surface of the samples can be seen. Both microscopic and macroscopic pores were observed (Fig. 4).

The chemical composition of the prepared samples determined by EDX analysis is summarized in Fig. 4 and Table 1. Iron and urea were used to prepare the samples. Since the urea was removed, only iron is expected to be present in the samples, with a small amount of carbon, since carbonyl iron powder was used during the preparation. The oxygen,

Fig. 1 Urea particles used as a space holder (a) and comparison of pure and Fe-coated urea particles (b)



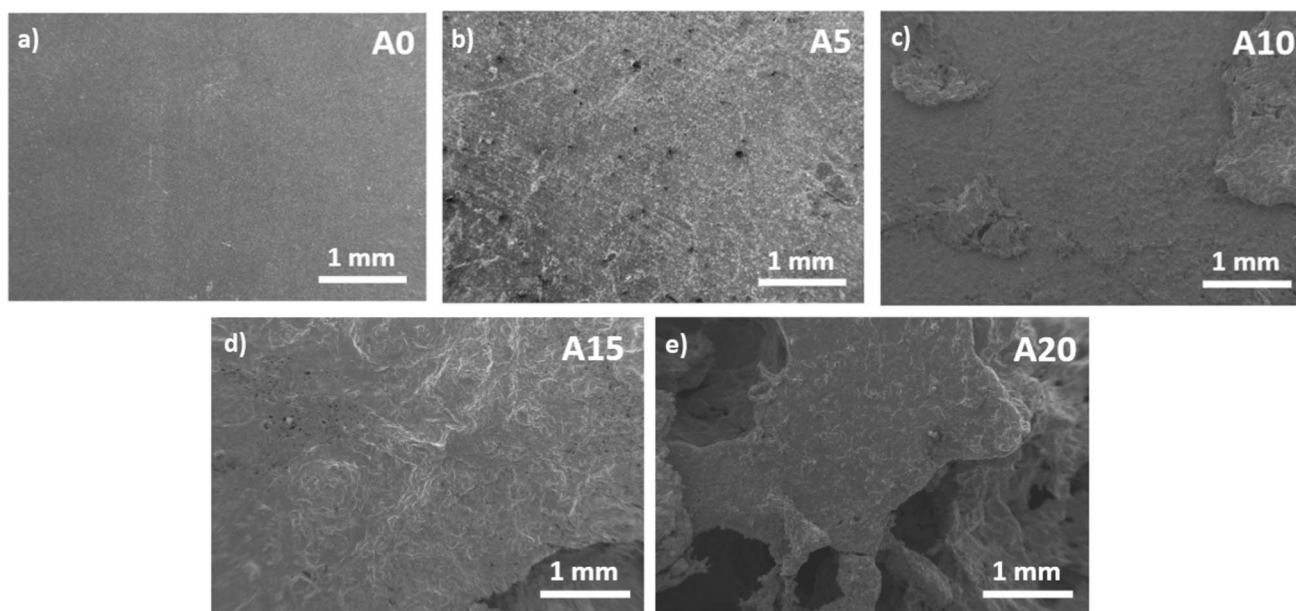


Fig. 3 SEM micrographs of the surface of the prepared samples with 0 (a), 5 (b), 10 (c), 15 (d), and 20 (e) urea space holder weight percentage

nitrogen, and carbon from the urea should be converted into a gaseous product by combustion. From the analyses in Fig. 4a–e and Table 1, it can be concluded that the urea was burned and evaporated from the samples. Low carbon content was found in every sample, including sample A0, where urea was not present. We assume that this is carbon coming from carbonyl iron powder as it is carbonylated.

Raman spectroscopy was performed to confirm the removal urea as a space holder. It is clearly seen from the Raman spectra on Fig. 5 that the urea was completely removed from the samples after sintering. The insert spectrum shows the zoom of the area of the spectrum of sintered samples in which the peaks were observed and, as can be seen, belonged to the iron oxides on the surface.

3.2 Mechanical properties

To study the mechanical properties, the dynamic resonant method was used to obtain the modulus of elasticity, the so-called Young's modulus. Because iron was used for the fabrication, the modulus of elasticity is assumed to be higher than that of bone. This was confirmed after the test and the results are summarized in Table 2. The A20 reached a value of 61.3 GPa. This is due to the large volume of pores and therefore the lack of material to stretch. In the future, it will be necessary to use a space holder with a smaller volume or space holder particles with a smaller diameter, as there is currently a small number of large pores in the sample. With

a smaller space holder, there would be more small pores in the sample, which would also improve the sample elasticity.

Young's modulus of cancellous bone varies depending on the location, orientation, and density of the bone. According to different studies, it can widely range from 0.01 to 9.8 GPa. The Young's modulus in the longitudinal direction of the compact bone is about 17 GPa, while in the transverse direction, it is about 12 GPa. Compared to Young's modulus of bones, the prepared samples are stronger and more durable [36].

3.3 Corrosion behaviour

It can be seen from Table 3 and Fig. 6 that the corrosion potential after sintering shifted towards more negative values with increasing content of urea used or number of pores. As a result, samples with a higher urea content and thus higher porosity are thermodynamically less resistant to corrosion. From Table 3, it follows that the corrosion rate increases with increasing mass fraction of the space holder used. The observed increase in the degradation rate indicates that the gradual increase in the number of pores leads to an increase in the surface area of the pores that are formed after urea removal.

It can be concluded that porous Fe materials prepared with a low content of space holder show an increase in the degradation rate compared to Fe material prepared without space holder, due to a larger surface area available for the electrolyte, i.e. on which corrosion can take place.

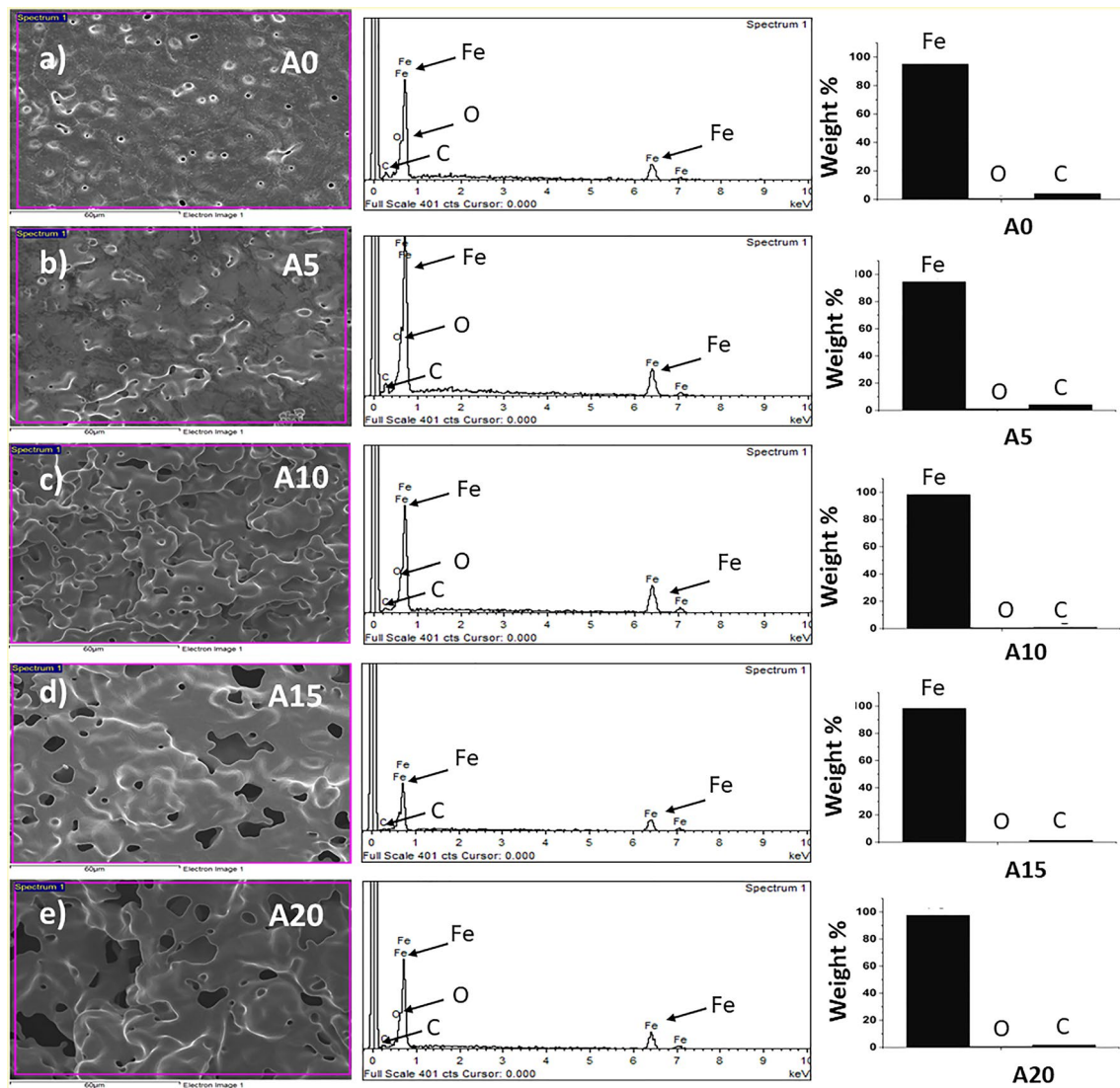


Fig. 4 SEM micrographs ($\times 1000$ magnification) and EDX analysis of iron foams with 0 (a), 5 (b), 10 (c), 15 (d), 20 (e) urea space holder weight percentage

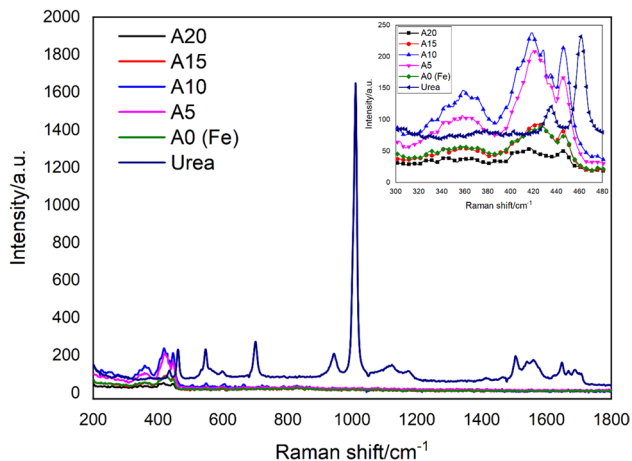
The presence of corrosion products on the surface of the samples after corrosion was studied by XRD analysis. XRD patterns shown in Fig. 7 revealed the presence of hematite ($\alpha\text{-Fe}_2\text{O}_3$) in samples with higher porosity [37]. With the decrease in the number of pores, the signal of hematite was lower, and the presence of hematite was not observed in the samples A0 and A5. A higher content of this corrosion product on the surface of the samples corresponds to a higher degradation rate of the samples prepared with a higher content of urea. XRD patterns also confirmed the presence of carbonyl iron in all the studied samples [38].

4 Discussion

Orthopaedic implants made of biodegradable porous metals are suitable candidates for repairing the damaged bones since their stiffness and porosity can be tuned. One of the main advantages of using degradable porous implants over non-porous ones is that cells can easily grow through their pores, which helps in the healing of bone tissue thus accelerating the osseointegration process [39]. In this work, we fabricated biodegradable porous Fe biomaterials with appropriate mechanical properties by cold-pressing and sintering using urea particles as space holders. Afterwards,

Table 1 EDX elemental analysis of the sample surface chemical composition

Sample	Element/wt%		
	Fe	O	C
A0	95.14	0.64	4.22
A5	94.59	1.23	4.18
A10	98.37	0.64	1.00
A15	98.44	0.00	1.56
A20	97.59	0.53	1.88

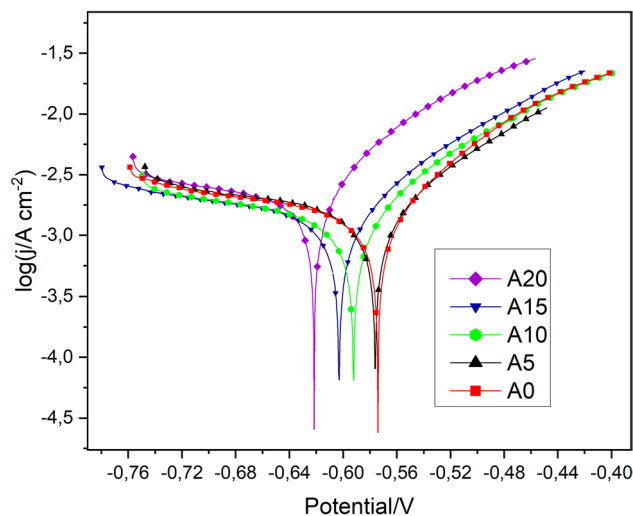
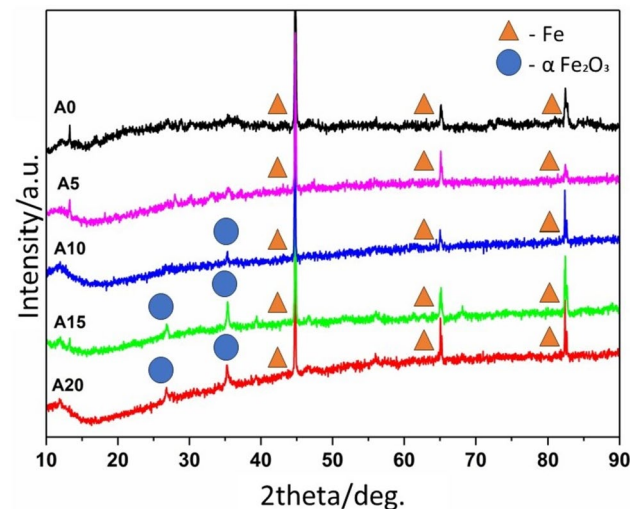
**Fig. 5** Raman spectra of the Fe and Fe-Ur samples after sintering**Table 2** Young's modulus measured values

Sample	E/GPa
A0	168.9
A5	119.3
A10	108.9
A15	104.9
A20	61.3

Table 3 Electrochemical properties measured in Hank's solution at 37 °C and pH=7.4 by potentiodynamic linear method

Sample	$j_{\text{corr}}/\mu\text{A cm}^{-2}$	E_{corr}/V	$CR/\text{mm year}^{-1}$
A0	1.65	-0.574	0.429
A5	2.20	-0.577	0.555
A10	2.02	-0.592	0.549
A15	1.15	-0.603	0.642
A20	0.59	-0.622	0.746

the samples were sintered at 1120 °C. The temperature 1120 °C was chosen since it is common sintering temperature for iron powder and this temperature is suitable for densifying the iron particles and achieving good mechanical properties. The dynamic resonant method showed that the samples can withstand higher tensile stresses than

**Fig. 6** Comparison of Tafel plots measured in Hank's solution at 37 °C and pH=7.4 for Fe-Ur samples**Fig. 7** XRD analysis of Fe-Ur porous samples after corrosion

bone and are therefore more elastic. As the urea content in the samples increased, the number of macroscopic and microscopic pores increased and, as a result, the value of Young's modulus also increased. The EDX analysis and Raman spectroscopy confirmed that the space holder particles were completely removed from the structure after sintering. The study of corrosion properties revealed that the sample A20 with the highest porosity exhibited the most negative corrosion potential value of -622 mV and the highest corrosion rate of 0.746 mm year⁻¹ among the prepared samples. Sample A0 without urea (lowest number of pores) corroded the slowest. Moreover, the corrosion rate of porous samples increases with the

increase in the number of pores. In comparison, a porous iron samples prepared from carbonyl iron powder by the impregnation of the polyurethane foam corroded at a rate of $0.045 \text{ mm year}^{-1}$, which is almost ten times slower than A0 sample with a corrosion rate of $0.429 \text{ mm year}^{-1}$ [40]. In another study, porous Fe scaffolds prepared by powder metallurgy techniques exhibited a corrosion rate of $0.04 \text{ mm year}^{-1}$ [41]. In study, where scaffolds were prepared via 3D printing, Fe scaffolds exhibited a corrosion rate of $0.065 \pm 0.030 \text{ mm year}^{-1}$ [42]. It follows that the samples prepared in this study achieve a much higher corrosion rate than the porous iron scaffolds prepared by different methods so far. The preparation of Fe porous biomaterials by powder metallurgy using urea as a space holder appears to be an affordable and simple way to tune the corrosion rate of these scaffolds, which was the aim of this work. Scaffolds prepared in this way still need to be further investigated mainly in terms of cytotoxicity and biocompatibility, which is decisive for their potential use as future orthopaedic implants.

5 Conclusions

Biodegradable porous Fe materials fabricated by powder metallurgy using urea particles as space holders represent a promising alternative biomaterial for the repairing of load-bearing bone defects in a cost-effective way. The tensile test of the prepared samples showed that the values of Young's modulus were much higher compared to the value of 17 GPa for bone. An electrochemical study of corrosion properties showed that the samples with higher number of pores (higher surface area) exhibited more negative corrosion potential values and corroded faster. Sample A20 with the highest porosity showed the most negative corrosion potential value (-622 mV) and the highest corrosion rate ($0.746 \text{ mm year}^{-1}$). In addition, a direct relationship between the amount of urea used in the preparation of samples and the number of pores formed in the samples after the removal of the urea was confirmed, which can be used to achieve the desired corrosion rate.

Author contributions VC contributed to investigation and writing—original draft; RG contributed to conceptualization, methodology, writing—review & editing, and funding acquisition; RM contributed to investigation and writing—original draft; OP contributed to investigation and writing—original draft; TS contributed to investigation and data analysis; MK contributed to investigation and data analysis; FK contributed to investigation; RO contributed to validation, supervision, writing—review & editing, and funding acquisition.

Funding Open access funding provided by The Ministry of Education, Science, Research and Sport of the Slovak Republic in cooperation with Centre for Scientific and Technical Information of the

Slovak Republic. This work was supported by the Slovak Research and Development Agency under the project APVV-20-0278, by the Operational Program for Research, Development and Education, co-funded by the European Union, within the framework of project no. CZ.02.2.69/0.0/0.0/18_053/0017879 entitled International mobility of UTB researchers in Zlín II and by the Development Agency, by the Ministry of Education, Youth and Sports of the Czech Republic (Project No. DKRVO RP/CPS/2022/005), by the Visegrad Grants from International Visegrad Fund. (Project No. 22310096) and by the Internal Research Grant of Faculty of Science of P. J. Šafárik University (VVGs-2023-2550).

Data availability Data are available on request from authors.

Declarations

Conflict of interest Authors declare no competing interests.

Open Access This article is licensed under a Creative Commons Attribution 4.0 International License, which permits use, sharing, adaptation, distribution and reproduction in any medium or format, as long as you give appropriate credit to the original author(s) and the source, provide a link to the Creative Commons licence, and indicate if changes were made. The images or other third party material in this article are included in the article's Creative Commons licence, unless indicated otherwise in a credit line to the material. If material is not included in the article's Creative Commons licence and your intended use is not permitted by statutory regulation or exceeds the permitted use, you will need to obtain permission directly from the copyright holder. To view a copy of this licence, visit <http://creativecommons.org/licenses/by/4.0/>.

References

- Hassan M et al (2022) Innovations in genomics and big data analytics for personalized medicine and health care: a review. *Int J Mol Sci.* <https://doi.org/10.3390/ijms23094645>
- Rabeeh VPM, Hanas T (2022) Progress in manufacturing and processing of degradable Fe-based implants: a review. *Progress Biomater* 11(2):163–191. <https://doi.org/10.1007/s40204-022-00189-4>
- Chandra G, Pandey A (2020) Biodegradable bone implants in orthopedic applications: a review. *Biocybern Biomed Eng* 40(2):596–610. <https://doi.org/10.1016/j.bbe.2020.02.003>
- Yavari SA, Castenmiller SM, Van Strijp JAG, Croes M (2020) Combating Implant Infections: shifting focus from bacteria to host. *Adv Mater.* <https://doi.org/10.1002/adma.202002962>
- Dhar Y, Han Y (2020) Current developments in biofilm treatments: wound and implant infections. *Eng Regen* 1:64–75. <https://doi.org/10.1016/j.engreg.2020.07.003>
- Ronin D, Boyer J, Alban N, Natoli RM, Johnson A, Kjellerup BV (2022) Current and novel diagnostics for orthopedic implant biofilm infections: a review. *APMIS* 130(2):59–81. <https://doi.org/10.1111/apm.13197>
- Thomas P (2014) Clinical and diagnostic challenges of metal implant allergy using the example of orthopaedic surgical implants. *Allergo J* 23(6):40. <https://doi.org/10.1007/s40629-014-0023-3>
- Reclaru L, Lerf R, Eschler P-Y, Meyer J-M (2001) Corrosion behavior of a welded stainless-steel orthopedic implant. *Biomaterials.* [https://doi.org/10.1016/S0142-9612\(00\)00185-X](https://doi.org/10.1016/S0142-9612(00)00185-X)
- Gorejová R et al (2022) Electrochemical behavior, biocompatibility and mechanical performance of biodegradable iron with

- PEI coating. *J Biomed Mater Res A* 110(3):659–671. <https://doi.org/10.1002/jbm.a.37318>
10. Jin W, Chu PK (2019) Orthopedic implants. In: *Encyclopedia of biomedical engineering*, vol 1–3. Elsevier, Amsterdam, pp 425–439
 11. Gorejová R, Haverová L, Oriňaková R, Oriňák A, Oriňák M (2019) Recent advancements in Fe-based biodegradable materials for bone repair. *J Mater Sci* 54(3):1913–1947. <https://doi.org/10.1007/s10853-018-3011-z>
 12. Li H, Zheng Y, Qin L (2014) Progress of biodegradable metals. *Progress Nat Sci: Mater Int* 24(5):414–422. <https://doi.org/10.1016/j.pnsc.2014.08.014>
 13. Al Sakkaf A, Januddi FS, Yusop AHM, Nur H (2022) Challenges in the use of Fe-based materials for bone scaffolds applications: perspective from in vivo biocorrosion. *Mater Today Commun* 33:104564. <https://doi.org/10.1016/j.mtcomm.2022.104564>
 14. Xing F et al (2022) Recent progress in Mg-based alloys as a novel bioabsorbable biomaterials for orthopedic applications. *J Magnes Alloys* 10(6):1428–1456. <https://doi.org/10.1016/j.jma.2022.02.013>
 15. Uppal G, Thakur A, Chauhan A, Bala S (2022) Magnesium based implants for functional bone tissue regeneration—a review. *J Magnes Alloys* 10(2):356–386. <https://doi.org/10.1016/j.jma.2021.08.017>
 16. Hussain M, Ullah S, Raza MR, Abbas N (2023) Recent developments in Zn-based biodegradable materials for biomedical applications. *J Funct Biomater*. <https://doi.org/10.3390/jfb14010001>
 17. Yang H et al (2020) Alloying design of biodegradable zinc as promising bone implants for load-bearing applications. *Nat Commun* 11(1):1–16. <https://doi.org/10.1038/s41467-019-14153-7>
 18. Gupta CP (2014) Role of iron (Fe) in body. *J Appl Chem* 7(11):38–46. <https://doi.org/10.9790/5736-071123846>
 19. Zoroddu MA, Aaseth J, Crisponi G, Medici S, Peana M, Nurchi VM (2019) The essential metals for humans: a brief overview. *J Inorg Biochem* 195:120–129. <https://doi.org/10.1016/j.jinorgbio.2019.03.013>
 20. Abbasi N, Hamlet S, Love RM, Nguyen NT (2020) Porous scaffolds for bone regeneration. *J Sci: Adv Mater Devices* 5(1):1–9. <https://doi.org/10.1016/j.jsamd.2020.01.007>
 21. Qin J, Chen Q, Yang C, Huang Y (2016) Research process on property and application of metal porous materials. *J Alloys Compd* 654:39–44. <https://doi.org/10.1016/j.jallcom.2015.09.148>
 22. Yin S, Zhang W, Zhang Z, Jiang X (2019) Recent advances in scaffold design and material for vascularized tissue-engineered bone regeneration. *Adv Healthc Mater*. <https://doi.org/10.1002/adhm.201801433>
 23. Hernandez JL, Woodrow KA (2022) Medical applications of porous biomaterials: features of porosity and tissue-specific implications for biocompatibility. *Adv Healthc Mater*. <https://doi.org/10.1002/adhm.202102087>
 24. Bagherifard A et al (2020) Improvement in osseointegration of tricalcium phosphate-zircon for orthopedic applications: an in vitro and in vivo evaluation. *Med Biol Eng Comput* 58(8):1681–1693. <https://doi.org/10.1007/s11517-020-02157-1>
 25. Alireza Hashemi S et al (2020) Micro-finite element model to investigate the mechanical stimuli in scaffolds fabricated via space holder technique for cancellous bone. *Int J Adv Des Manuf Technol* 13(1):51–58
 26. Sahmani S, Saber-Samandari S, Khandan A, Aghdam MM (2019) Influence of MgO nanoparticles on the mechanical properties of coated hydroxyapatite nanocomposite scaffolds produced via space holder technique: fabrication, characterization and simulation. *J Mech Behav Biomed Mater* 95:76–88. <https://doi.org/10.1016/j.jmbbm.2019.03.014>
 27. Abdollahi M, Najafinezhad A, Ghayour H, Saber-Samandari S, Khandan A (2017) Preparing diopside nanoparticle scaffolds via space holder method: simulation of the compressive strength and porosity. *J Mech Behav Biomed Mater* 72:171–181. <https://doi.org/10.1016/j.jmbbm.2017.05.004>
 28. Salmani MM, Hashemian M, Khandan A (2020) Therapeutic effect of magnetic nanoparticles on calcium silicate bioceramic in alternating field for biomedical application. *Ceram Int* 46(17):27299–27307. <https://doi.org/10.1016/j.ceramint.2020.07.215>
 29. Torres Y, Lascano S, Bris J, Pavón J, Rodríguez JA (2014) Development of porous titanium for biomedical applications: a comparison between loose sintering and space-holder techniques. *Mater Sci Eng C* 37(1):148–155. <https://doi.org/10.1016/j.msec.2013.11.036>
 30. Conde Y et al (2006) Replication processing of highly porous materials. *Adv Eng Mater* 8(9):795–803. <https://doi.org/10.1002/adem.200600077>
 31. Fayazfar H et al (2018) A critical review of powder-based additive manufacturing of ferrous alloys: process parameters, microstructure and mechanical properties. *Mater Des* 144:98–128. <https://doi.org/10.1016/j.matdes.2018.02.018>
 32. Ali S et al (2022) Microstructure and mechanical properties of modified 316L stainless steel alloy for biomedical applications using powder metallurgy. *Materials (Basel)*. <https://doi.org/10.3390/ma15082822>
 33. Oriňaková R, Gorejová R, Kráľová ZO, Petráková M, Oriňák A (2021) Novel trends and recent progress on preparation methods of biodegradable metallic foams for biomedicine: a review. *J Mater Sci* 56(25):13925–13963. <https://doi.org/10.1007/s10853-021-06163-y>
 34. Wei S, Ma JX, Xu L, Gu XS, Ma XL (2020) Biodegradable materials for bone defect repair. *Mil Med Res*. <https://doi.org/10.1186/s40779-020-00280-6>
 35. Hrubovčáková M, Kupková M, Džupon M (2016) Fe and Fe-P foam for biodegradable bone replacement material: morphology, corrosion behaviour, and mechanical properties. *Adv Mater Sci Eng*. <https://doi.org/10.1155/2016/6257368>
 36. Zhu S et al (2022) Bioinspired nacre-like PEEK material with superior tensile strength and impact toughness. *RSC Adv* 12(24):15584–15592. <https://doi.org/10.1039/d2ra00667g>
 37. Xu S, Habib AH, Gee SH, Hong YK, McHenry ME (2015) Spin orientation, structure, morphology, and magnetic properties of hematite nanoparticles. *J Appl Phys*. <https://doi.org/10.1063/1.4914059>
 38. Srga V, Maiorov M, Cvetkovs A, Krumina A, Popov AI (2018) Fabrication and characterization of magnetic FePt nanoparticles prepared by extraction-pyrolysis method. *Chemija* 29(2):109–114. <https://doi.org/10.6001/chemija.v29i2.3713>
 39. Liu CZ, Czernuszka JT (2007) Development of biodegradable scaffolds for tissue engineering: a perspective on emerging technology. *Mater Sci Technol* 23(4):379–391. <https://doi.org/10.1179/174328407X177027>
 40. Gorejová R et al (2020) In vitro corrosion behavior of biodegradable iron foams with polymeric coating. *Materials (Basel)* 13(1):184. <https://doi.org/10.3390/ma13010184>
 41. Dargusch MS et al (2019) Exploring the role of manganese on the microstructure, mechanical properties, biodegradability, and biocompatibility of porous iron-based scaffolds. *ACS Biomater Sci Eng*. <https://doi.org/10.1021/acsbomaterials.8b01497>
 42. Chou DT, Wells D, Hong D, Lee B, Kuhn H, Kumta PN (2013) Novel processing of iron-manganese alloy-based biomaterials by inkjet 3-D printing. *Acta Biomater* 9(10):8593–8603. <https://doi.org/10.1016/j.actbio.2013.04.016>

Authors and Affiliations

V. Čákyová¹ · R. Gorejová^{1,2}  · R. Macko¹ · O. Petruš³ · T. Sopčák³ · M. Kupková³ · F. Kaľavský¹ · R. Oriňaková^{1,2} 

✉ R. Gorejová
radka.gorejova@upjs.sk; gorejova@utb.cz

V. Čákyová
viktoria.cakyova@student.upjs.sk

R. Macko
rastislav.macko@student.upjs.sk

O. Petruš
opetrus@saske.sk

T. Sopčák
tsopcak@saske.sk

M. Kupková
mkupkova@saske.sk

F. Kaľavský
frantisek.kalavsky@upjs.sk

R. Oriňaková
renata.orinakova@upjs.sk; orinakova@utb.cz

¹ Department of Physical Chemistry, Faculty of Science,
Institute of Chemistry, Pavol Jozef Šafárik University
in Košice, Moyzesova 11, 040 01 Košice, Slovakia

² Centre of Polymer Systems, University Institute, Tomas Bata
University in Zlín, Třída Tomáše Bati 5678, 76001 Zlín,
Czech Republic

³ Institute of Material Research, Slovak Academy of Sciences,
Watsonova 47, 040 01 Košice, Slovakia